Natural Resources Canada | Ressources naturelles Canada

GEOLOGICAL SURVEY OF CANADA
OPEN FILE 8718

# A comprehensive earthquake catalogue for the Fort St. John–Dawson Creek region, British Columbia, 2017–2018

R. Visser, H. Kao, B. Smith, C. Goerzen, B. Kontou, R.M.H. Dokht, J. Hutchinson, F. Tan, and A. Babaie Mahani

2020

Canada

**GEOLOGICAL SURVEY OF CANADA**
**OPEN FILE 8718**

# A comprehensive earthquake catalogue for the Fort St. John–Dawson Creek region, British Columbia, 2017–2018

**R. Visser[1], H. Kao[1,2], B. Smith[1,3], C. Goerzen[1,2], B. Kontou[1], R.M.H. Dokht[1], J. Hutchinson[1,2], F. Tan[1,2], and A. Babaie Mahani [1,4]**

[1]Geological Survey of Canada, 9860 West Saanich Road, Sidney, British Columbia V8L 4B2
[2]School of Earth and Ocean Sciences, University of Victoria, 9882 Ring Road, Victoria, British Columbia V8P 3E6
[3]Department of Physics, McGill University, 3600 Rue University, Montréal, Quebec H3A 2T8
[4]Geoscience BC, 1101-750 West, Pender Street, Vancouver, British Columbia V6C 2T7

## 2020

© Her Majesty the Queen in Right of Canada, as represented by the Minister of Natural Resources, 2020

Information contained in this publication or product may be reproduced, in part or in whole, and by any means, for personal or public non-commercial purposes, without charge or further permission, unless otherwise specified.
You are asked to:
- exercise due diligence in ensuring the accuracy of the materials reproduced;
- indicate the complete title of the materials reproduced, and the name of the author organization; and
- indicate that the reproduction is a copy of an official work that is published by Natural Resources Canada (NRCan) and that the reproduction has not been produced in affiliation with, or with the endorsement of, NRCan.

Commercial reproduction and distribution is prohibited except with written permission from NRCan. For more information, contact NRCan at nrcan.copyrightdroitdauteur.rncan@canada.ca.

Permanent link: https://doi.org/10.4095/326015

This publication is available for free download through GEOSCAN (https://geoscan.nrcan.gc.ca/).

**Recommended citation**
Visser, R., Kao, H., Smith, B., Goerzen, C., Kontou, B., Dokht, R.M.H., Hutchinson, J., Tan, F., and Babaie Mahani, A., 2020. A comprehensive earthquake catalogue for the Fort St. John–Dawson Creek region, British Columbia, 2017–2018; Geological Survey of Canada, Open File 8718, 1 .zip file. https://doi.org/10.4095/326015

Publications in this series have not been edited; they are released as submitted by the author

## Abstract

To gain a better understanding of induced seismicity in northeastern British Columbia, we conducted an analysis of seismic data to locate earthquakes that occurred within the area of 55.5°N–56.3°N and 119.8°W-121.2°W for the years of 2017 and 2018. This catalogue contains earthquakes that were detected and located using a combination of manual analysis and a semi-automated process utilizing the newly developed Seismicity-Scanning based on Navigated Automatic Phase-picking (S-SNAP) algorithm (Tan et al., 2019). There were two major seismic station deployments within the study area during the study period which significantly increased our ability to locate small earthquakes ($M_L$ <1.5). Our dataset consisted of continuous seismic waveforms from a total of 52 stations operated by various organizations in the region. A total of 10,692 events were identified, located, and had solutions which passed our quality control criteria. For the same period and area, the Canadian National Seismograph Network (CNSN) routine catalogue 71 events – all are included in this study. In this report, we describe in detail both the manual location procedures and our implementation of S-SNAP. The earthquake catalogue, picking information, and magnitude information are included in separate files and can easily be joined using the earthquake origin IDs. The total number of events in 2017 and 2018 are 5779 and 4914, respectively. The overall magnitude of completeness of our catalogue is $M_L$ ~1.5 for the period of 2017-01 through 2017-06, when there were only 2 stations within the study area, and ~$M_L$ 1.0 when there were 10 or more stations in the area from 2017-07 onwards.


## 1. Introduction

The study area in northeastern British Columbia (BC), which covers an area between Fort St John and Dawson Creek, BC, is part of the Western Canada Sedimentary Basin (WCSB). Although oil and gas production has been decreased due to the economic recession in recent years, the presence of desirable condensates from several hydrocarbon-

bearing formations enabled this region to remain active during 2017 and 2018. Historically the WCSB was not considered a seismically active region, and the vast majority of significant earthquakes ($M \geq 4$) in western Canada occurred near the coast due to plate boundary processes. Since northeastern BC and western AB are situated further than 800 km from the western boundary of the North American plate, previous seismicity in the area is consistent with an intraplate tectonic setting.

Although extraction of hydrocarbons from conventional resources in WCSB started in the 1950's, unconventional resources remained undeveloped until the turn of the century, when advances in hydraulic fracturing made it possible to extract hydrocarbon from low-permeable reservoirs (National Energy Board, 2013). The Heritage Montney field, which is the main field within the focus of this study, is one of several major shale gas plays within the WCSB. The field makes up the southeasternmost section of the Montney Trend in BC, which extends from northeastern British Columbia (BC) and into Western Alberta (Johnson, 2008). Several studies have shown a correlation between the sharp increase in regional seismicity in the WCSB and injection operations related to the development of unconventional hydrocarbons (e.g., Atkinson, et al. 2016, Ellsworth 2013, Farahbod, et al. 2015b, Keranen, et al. 2014). This increase of injection-induced earthquakes (IIE) was observed in recent years as the unconventional oil and gas development in northeastern BC and western AB significantly expanded (Atkinson, et al. 2016, Farahbod, et al. 2015a, Schultz, et al. 2017).

In order to obtain the most complete seismic pattern for the study of IIE and the associated seismic hazard, the Induced Seismicity Research (ISR) Project, established under the Environmental Geoscience Program, decided to examine seismic records collected by regional and local seismograph networks from 1 January 2017 through 31 December 2018. This report summarizes the output and our effort to establish the most comprehensive earthquake catalogue for the Fort St. John–Dawson Creek area.

## 2. Data and Analysis

Our study area corresponds to the latitude and longitude ranges of 55.5°N–56.3°N and 119.8°W–121.2°W, respectively. The area had a densification of seismic stations over the study period which significantly aided the detection of earthquakes with lower magnitudes.

From January through June 2017, the only stations within the study area were NBC4 and NBC7. In July 2017, McGill University installed 8 broadband seismograph stations (FDSN network code XL) which was later expanded to a 9-station network in June 2018. Furthermore, in late September 2018, NRCan, the BC Oil and Gas Commission (BCOGC), and McGill University initiated a collaboration that included the deployment of 7 additional stations (FDSN network code 1E) in northeastern BC (Figure 1, Table 1). We run S-SNAP and conduct manual analysis on separate time periods. To have confidence to do this, we compared manual and S-SNAP earthquake detections and locations for the month of July 2017. Our comparison result indicates that S-SNAP missed just two of the 197 $M_L \geq 1.0$ events (each event with 10 or more manually picked arrivals). None of the $M_L \geq 1.2$ events (with 12 or more manually picked arrivals) were missed by S-SNAP.

## 2.1 Data Pipeline

We designed and followed a data processing pipeline in order to ensure the catalogue was created uniformly for the processes of earthquake detection and analysis using both manual locations and S-SNAP. Each method has a similarly structured data pipeline, but due to differences in data processing, they follow different quality control procedures to ensure the final catalogue consists solely of high-quality events (Figure 2). In order to highlight the key similarities and differences in each stage of analysis, processes are compared in the sections below.

### 2.1.1 Event Detection

**Manual:** The analyst visually scanned a series of waveforms using the Antelope module *dbpick*, running inside of *dbloc2*, with a 2-20 Hz integrated bandpass filter. When an event was recognized, the analyst added the arrivals of seismic phases accordingly.

**S-SNAP:** To prepare for S-SNAP, waveforms within the desired time windows were initially filtered with a 2–10 Hz bandpass filter. The study area was divided into a grid nodes and the source-scanning was done at one-second time steps. For each node at each timestep, the station-to-node travel times were used to identify the corresponding time windows on individual waveforms. Waveform amplitudes and kurtosis statistic values within the

corresponding time windows were multiplied together to give the "brightness" of that node-time pair. If the node and time correspond to the location and origin time of a true earthquake, then its brightness value is expected to be high because of the coherent arrivals of seismic phases. In general, the location of a seismic source can be easily recognized from a brightness map as a clear bright spot (Figure 3). We set a threshold for the maximum brightness value to declare the existence of an event. Detailed technical setup of S-SNAP is given in Section 2.2.

### 2.1.2 Phase Identification

**Manual:** Analysts used the *dbpick* Antelope module and a variety of frequency filters to visually inspect waveforms and identify the phase arrival times. The picked arrival times were then stored in the Antelope system.

**S-SNAP:** S-SNAP identified phases by scanning each channel's waveform during the time window indicated by the corresponding node with the highest brightness value. P picks were determined by finding the kurtosis rate that first exceeded a given threshold value on the vertical channel — 0.9 for this study. S picks were determined in the same way with the additional constraints that they must have occurred later in time than P arrivals (if present) using the horizontal channel with the highest amplitude.

### 2.1.3 Preliminary Location

**Manual:** Event locations were generated by selecting arrivals within the Antelope module *dbloc2,* then locating them with the location model, *genloc*.

**S-SNAP:** Picked arrival times were taken from the phase identification step to construct equal differential time (EDT) surfaces that, in turn, were used in a grid search to determine the preliminary location of a seismic source (i.e., the MAXI approach, Font et al., 2004). Specifically, the hypocentre was identified as the location with the maximum intersection of EDT surfaces.

### 2.1.4 Finalized Locations

**Manual:** Event locations were visually inspected a second and final time

before picks and locations were finalized.

**S-SNAP:** The output of S-SNAP was a Python Pickle file containing a dictionary of events and the associated phase information included time, phase, station, and channel. All events with 6 or more quality phases had locations and phase picks manually reviewed using the Waveform Viewer GUI (Figure 4). If a visually inspected event was considered a false detection, the event was discarded; if the event was real but had any mistimed or false arrivals it was marked for manual relocation, otherwise the event was considered real with good phase arrivals and included in the final catalogue. Events marked for manual relocation had arrivals and preliminary origins input to a new Antelope database where they proceeded through the Antelope data pipeline. The densification of stations within the study area significantly improved the effectiveness of S-SNAP. For April – June 2017 when only limited numbers of stations were available, the mean magnitude of events located by S-SNAP was 1.5 ($M_L$). The mean magnitude improved to 0.9 ($M_L$) for January – December 2018 (4777 events).

### 2.1.5 Magnitude Determination

**Manual and S-SNAP:** All approved events and their details from both manual and S-SNAP located events were transferred to a new Antelope database to have magnitudes processed uniformly at one time. We used the Antelope function *evproc* to calculate station magnitudes on the vertical channel rather than the horizontal channels in order to be uniform with the magnitude values determined by CNSN. For our catalogue, local magnitude ($M_L$) was determined by taking the median value of station magnitudes.

### 2.1.6 Magnitude Correction

**Manual and S-SNAP:** Mahani & Kao (2019) reported a systematic bias in the $M_L$ calculation for regional earthquakes in northeastern BC when the original Richter distance correction table is used. Such a bias is mainly due to the inappropriate correction to account for the amplitude attenuation with distance. In this study, we first applied an amplitude correction to each

station based on its hypocentral distance according to the formula proposed in Mahani & Kao (2019). We then estimated the statistical differences between the magnitude values obtained at individual stations and the final event magnitude (Figure 5), which were then used as magnitude correction factors for each station (Table 2). The magnitude correction step is discussed further in section 2.8.

#### 2.1.7 Aggregation

**Manual and S-SNAP:** To combine the data from separate catalogues, we removed possible duplicate events, sorted events by time, and re-indexed the origins. The resulting catalogue has separate tables for origins, arrivals, and magnitudes which respectively are Appendix 1, 2, and 3 of this report.

### 2.2 S-SNAP Setup

Both S-SNAP and Antelope had a number of key similarities and differences in their setup processes, illustrated in Figure 6. These parameters and the decisions made for our implementation of S-SNAP are detailed below; details for the set-up of Antelope are discussed in Section 2.3 of this report.

**2.2.1 Station Selection:** When possible, only stations inside the study area were selected for use. If there was not a minimum of 10 stations within the study area, then the 10 closest stations to the study area were used. The decision to include only the very closest stations was made following observations that when stations at greater distances (or further than 50 km outside the study area) were added to the analysis, both the number of arrivals and detected events would often decrease. Due to the simple 1D velocity model used in this study, more distant stations have — on average — greater travel-time residuals than closer stations, and as a result are more likely to highlight incorrect nodes in the S-SNAP brightness function. An incorrect node may lead to scanning for phases in the time window when there are no phases. This would result in the event to be discarded in case the phase count threshold of 6 is not satisfied. We were able to obtain the best results when only stations within the study area were included.

**2.2.2 Instruments:** In the version of S-SNAP used for this study, only multi-channel broadband stations operating at 100 samples/second could be used. All stations in the study area met this criterion.

**2.2.3 Grid Nodes:** We selected grid nodes dividing the latitude and longitude range of the study area into 2.5 km intervals. Since induced earthquakes in this area are shallow and depth resolution is poor for shallow events, we set a constant node depth of 2.5 km.

**2.2.4 Software and Hardware Configuration:** The Python implementation of S-SNAP created by Tan et al. (2019) was installed and tested on two MacOS High Sierra systems.

**2.2.5 Event Detection:** S-SNAP scanned continuous waveforms for event detection. All waveforms were filtered with a 2–10 Hz bandpass filter. The preliminary scanning was done with a three second time window moving at one second intervals. The brightness value at each grid node was calculated as the product of the maximum kurtosis rate value of the P wave and the maximum kurtosis rate value for the S wave multiplied by the product of the mean amplitude of the P wave and the mean amplitude of the S wave. These brightness values were used to create the brightness maps for each time step. The brightness maps were then used to determine the precise arrival times on individual station waveforms in the next step. We refer readers to Tan et al. (2019) for more theoretical and technical details.

**2.2.6 Phase Picking**: The preliminary locations from the brightness map are used to calculate the theoretical arrivals for P and S phases with a surrounding time window of ±1.5 seconds. Arrivals were then scanned for onsets using the kurtosis statistic; values were required to exceed 0.9 in order to be selected.

**2.2.7 Event Location:** The MAXI location method is built into S-SNAP and was used to determine event locations. Events that had a minimum of 6 associated phases, each phase below the allowable travel time residual of 0.5s, were kept as candidates for further review.

**2.2.8 Travel Time Tables:** The times required for seismic waves to travel from

each node to each station was pre-calculated for both P and S phases based on the velocity model CN01, which is broken down in greater detail in Section 2.4.1. We used the resulting travel time tables to determine the time window that should be included in the brightness calculation at individual stations.

## 2.3 Antelope Setup

**2.3.1 Station Selection:** All local and regional stations surrounding the study area were included in this study. The 52 stations which had picks determined on them are included in the station list given in Table 1.

**2.3.2 Instruments:** Both broadband and short-period stations with different sample rates could be included in manual locations.

**2.3.3. Software and Hardware Configuration:** Two MacOS computers and one Linux box with Centos 7 were set up to use Boulder Real Time Technologies' (BRTT) Antelope software package (version 5.7). Antelope was set up to use the velocity model CN01 and limited to a depth range of 0-30 km. Waveform filters for scanning and locations were set up to include: 1 HP, 3 HP, 1-5 BP, 1-10 BP, 2-20 BP, 2-20 integrated BP, or 5-20 BP.

**2.3.4 Event Detection:** Phase detection for manual locations was performed through visual examination of waveforms using the Antelope module *dbpick*, running inside of *dbloc2*, and using a 2-20 Hz integrated bandpass filter.

**2.3.5 Magnitude Settings**: The calculation of local magnitude ($M_L$) is based on the maximum amplitude recorded on the vertical channel. Due to the generally smaller size of IIE, we had to adjust the threshold of the signal-to-noise ratio (SNR) from 3.0 to 1.5. The magnitude calculation was set to take the median value as opposed to the mean to be less sensitive to outliers.

## 2.4 Study Settings:

For the data pipeline there are a number of settings that must be chosen to ensure good results.

**2.4.1 Velocity Model Settings**: Both S-SNAP and Antelope used the same velocity model - the two-layer velocity model CN01. This model is also the one used by CNSN in routine location of regional earthquakes in the WCSB. In this model, depths from 0 to 36 km have the corresponding *P* and *S* velocities of 6.2 km/s and 3.57 km/s, respectively. For depths below 36 km, *P* and *S* velocities are 8.2 km/s and 4.7 km/s, respectively.

**2.4.2 Hypocentre Error Distance Filter**: Events for S-SNAP and manual locations were limited to a depth range of 0–30 km. Approximately 90% of event solutions in the catalogue are shallower than 5 km, while 98% of solutions fall within 10 km depth. Locations were restricted to the bounds of the study area, and any events outside of the given criteria were removed from the catalogue.

## 2.5 Building the Waveform Database

Seismic station details and continuous waveforms in miniSEED format were obtained from the Incorporated Research Institutions for Seismology (IRIS) by using the MassDownloader function of ObsPY. Station and waveform information that was not available from IRIS was supplemented by data available from NRCan's Canadian Hazard Information Service (CHIS). Waveforms obtained through IRIS were downloaded as daily files, then sorted into folders and processed chronologically. Station data from IRIS and CHIS were consolidated into a master station file. Antelope databases were finalized by creating a descriptor file, which pointed Antelope towards the master station table and the corresponding year of waveform data. S-SNAP databases were finalized by the creation of a station file which included the network, station, channel, location, and elevation information for each station to point the program to the proper file names.

## 2.6 Manual Analysis Using Antelope

For this report, we manually searched for seismic events in over 9 months of waveform data. To conduct this analysis for 52 stations, the vast majority of which had 3 channels, was a very time intensive task. To effectively complete the analysis, the process is split into two main stages – scanning and location. During the scanning stage, the analyst

manually searched waveforms for earthquake signals. When earthquakes were found, rough phase selections were made that would be finalized during the location stage. While scanning, all available channels were visible, with 0.5–5 minutes of each channel's waveform data visible at any one time. This short time window allowed the analyst to confidently scan all traces on the screen for earthquake phases before advancing the time window. Earthquake phases included in the catalogue were: *P*, *S*, *Pn*, *Pg*, *Sn*, and *Sg*. P and S phases were selected for stations within 150 km of the origin. For stations with an epicentral distance beyond 150 km from the origin, the *Pn*, *Pg*, *Sn*, and *Sg* phases were used. Two main filters were used during scanning to help identify seismic signals from local and regional events, as recommended by senior CNSN earthquake analysts; the 2-Hz high-pass integrated filter was used during general scanning to remove unwanted low frequency noise, while the 1–5-Hz band-pass filter was used to make phase picks on distant stations or stations with noise at higher frequencies. After the initial detection and location was performed by Antelope and S-SNAP, we conducted a final review in Antelope to ensure that the timing of phase picks is correct and that no events had been missed. We found that roughly 50% of the 4882 S-SNAP events had at least one arrival time that needed manual correction by an analyst in Antelope.

## 2.7 Comparison to the CNSN Earthquake Database

A small number of the seismic events found in this study were also reported in the CNSN Earthquake Database, the authority of earthquake locations within Canada. Having the same earthquakes in both catalogues gave us the opportunity to verify the accuracy of our solutions. For the same time period and area as our study, the CNSN Earthquake Database had 71 events, each of which is contained in our catalogue. The average distance for matching locations between catalogues is 3.2km. Since the XL and 1E networks are not included in CNSN routine location analysis, it probably can explain any location discrepancies. For periods prior to the XL and 1E network deployments, the small differences in location can be explained by possible uncertainties due to different station density and azimuthal coverage used in the location process.

## 2.8 Magnitude Correction

In routine earthquake locations by the CNSN, the original local magnitude calculation method that was developed for southern California (Richter, 1935, 1958) is used. As a result, different attenuation characteristics between WCSB and southern California lead to uncertainty in the magnitude calculation for earthquakes in our study area. In recent years, there have been two specific studies focusing on this issue (Yenier, 2017; Mahani & Kao, 2019). For the purposes of this study, we first implemented the amplitude correction according to the hypocentral distance as proposed in Mahani & Kao (2019). In order to further reduce the problem of systematic bias for the magnitude values derived from the peak amplitudes at individual stations relative to the event magnitude, we calculated the mean difference between the distance-corrected event magnitudes and the distance-corrected station magnitudes to compile the station correction factors for all stations used in this study (Figure 5 and Table 2). After applying both amplitude correction (mainly due to hypocentral distance) and station correction (mainly due to individual site effects), we obtained the final corrected magnitude value for each event by choosing the median of the corrected station magnitudes. The application of individual station correction factors successfully reduced the average station magnitude variance from 0.23 to 0.18. We present uncorrected magnitude, corrected magnitude, and amplitude information in the final catalogue.

### 2.9 Quality Control

In order to produce an earthquake catalog with only high-quality solutions, location boundaries were implemented at the margins where the seismic station density was lower and, correspondingly, the magnitude of completeness was worse than the study area. Earthquakes were only included the catalogue if they fell inside the latitude and longitude ranges of 55.5°N-56.3°N and 119.8°W-121.2°W, respectively. Events were kept if the length of their major axis error ellipse was less than 10 km. Approximately 99% of events had major axis errors less than 5 km, and ~91% had errors less than 2 km. For events detected and located by S-SNAP, we require that each of them must have a minimum of 6 associated phases and each phase must have a travel time residual less than 0.5 s. Consequently, the corresponding location error should be much less than the 10 km major axis error cut-off criterion. We have conducted an experiment to verify the small location

errors of S-SNAP solutions. When events with 6 phases were located using *genloc*, the median hypocentre major axis error is only 0.59 km with a maximum value of 6.81 km.

After earthquake locations were finalized, travel-time residuals for each observed phase were calculated based on the predicted arrival time by the Antelope program *genloc* (Pavlis, et al., 2004). The standard deviation of travel time residuals (SDOBS) for each earthquake solution computed by Antelope was determined by taking the square root of the sum of the squares of the time residuals, divided by the number of arrivals used in a solution minus either 4 (if depth is allowed to be free) or 3 (if depth is fixed). The max allowable SDOBS threshold was set at 1.0 s, and only events meeting this criterion are included in the final catalogue. Approximately 98% of our final solutions using Antelope have SDOBS less than 0.6 s.

For a magnitude to be determined for a station, the vertical channel was required to have an SNR that exceeded 1.5; events without any stations above the SNR threshold had no magnitude and were not included in the final catalogue.

## 3. Result

In focusing our efforts on seismic events limited to a small, roughly square area, (~88 km in the east-west direction x 89 km in the north-south direction) in northeastern BC from January 2017 through December 2018, we managed to find a total of 10704 events (Figure 7). The earthquake catalogue has events that match each of the 71 events reported in the CNSN Earthquake Database for the same period, with an average distance of 3.2 km between matching event epicenters. For CNSN solutions, the XL and 1E network were unused, likely accounting for any location discrepancies since these networks are the closest and thus most useful for detecting and locating seismicity in the study area.

We adopted the method proposed by Wiemer & Wyss (2000) to estimate the magnitude of completeness. There are two magnitudes of completeness for the two different time periods separated by the deployment of 9 XL array stations to our study area: The pre-deployment magnitude of completeness from January 2017 through July 2017 is estimated to be 1.5 ($M_L$), whereas the post deployment period from July 2017 to the end of 2018 is estimated to be 1.0 ($M_L$) (Figure 8). There was only 1 earthquake within the study area with a magnitude greater than 4 — a $M_w$ 4.5 event that occurred on 30 November 2018. Relative

to this earthquake there were two aftershocks with $M_L \geq 3$: first a $M_L$ 3.0 and secondly a $M_L$ 3.9; both on the same day as the main shock.

The distribution of seismicity shows a clear preference. Earthquakes tend to tightly cluster temporally and spatially, and generally occur in a northwestern - southeastern trend. Earthquakes in 2017 and 2018 both show this trend, though there are also sporadic clusters in different areas of each year. It is beyond the scope of this report to determine the exact causes of seismicity, but clusters of events are highly likely to be associated with industrial activities and fault structures in the area. Within the study area, clusters of local seismicity coincided remarkably well with areas of unconventional oil and gas development, most commonly hydraulic fracturing in the Montney Trend within the WCSB. Seismicity is in the area of, and could be correlated with, the complex fault structures of the Dawson Creek Graben Complex (DCGC), which includes the Fort St John Graben. The temporal distribution of seismicity also varies significantly throughout the study period. For example, it is clear from a plot of number of earthquakes per month, that the network performance was greatly improved from July 2017 onwards following the deployment of the XL seismic array (Figure 9).

It is evident that more events were detected during manually located portions of the catalogue than with S-SNAP. When we compared earthquake rates from periods located manually vs periods located by S-SNAP (Figure 10) there were nearly 3 times as many events per month for the period of 1 January 2017 – 31 March 2017, which was located manually, than during the period of 1 April 2017 – 30 June 2017, which was located by S-SNAP. The same trend can be seen through the comparison of number of earthquakes per month for the period of July 2017 - Dec 2017 and January 2018 - December 2018, with more than double the number of events per month located manually than via S-SNAP. This could be due to a number of reasons, one of which is the fact that S-SNAP requires a minimum of 6 phase picks from scanning with one filter in order to find an event versus the minimum of 3 phases required by analysts with a whole suite of filters using Antelope. Supporting this idea, there are over 1,000 events in the catalogue located by the analyst with fewer than 6 phases. These 1,000 events cannot account for the entire difference in the rate of seismicity for periods using different methods though. A year over year comparison showed that the average $M_L$ remained close to constant, from 0.91 in 2017, to

0.90 in 2018. The number of earthquakes detected each year decreased from 5779 in 2017 to 4914 in 2018 likely because of the key differences between S-SNAP and manual locations, which we have already discussed but we also must acknowledge the possibility that there were fewer active oil and gas operations during 2018 or that operations were conducted in areas less prone to induced seismicity leading to lower rates of induced seismicity.

Because of the deployment of twelve new stations in 2017 and 2018, we were able to significantly improve on the completeness of our previously published earthquake catalogue for 2014-2016 which included the same area (Visser et al., 2017). The previous catalogue covers a significantly larger area with 4,916 events and a magnitude of completeness of $M_L$ 1.8, whereas this new catalogue has 10,692 events and a completeness of $M_L$ ~1.0 for the majority of the study period.

## Acknowledgements

We are thankful to agencies responsible for the operation and maintenance of the seismograph networks in and around our study area, including CNSN, RV, 1E, XL, and YO. Comments and critical review by Taimi Mulder are very much appreciated. This study is partially supported by the ecoEnergy Innovation Initiative, the Office of Research and Development of NRCan, the Energy Innovation Program, and the Environmental Geoscience Program of NRCan.

## References

Atkinson, G. M., Eaton, D. W., Ghofrani, H., Walker, D., Cheadle, B., Schultz, R., … Kao, H. (2016). Hydraulic Fracturing and Seismicity in the Western Canada Sedimentary Basin. *Seismological Research Letters*, *87*(3), 631–647, doi:10.1785/0220150263.

BC Oil & Gas Commission. (2016). British Columbia's Oil and Gas Reserves and Production Report. Retrieved from https://www.bcogc.ca/node/14704

Ellsworth, W. L. (2013). Injection-Induced Earthquakes. *Science*, *341*(July), 1–8.

Farahbod, A. M., Cassidy, J. F., Kao, H., & Walker, D. (2014). Collaborative Studies of Regional Seismicity in Northeast British Columbia. *CSEG Recorder*, *39*(9), 40–44.

Farahbod, A. M., Kao, H., Cassidy, J. F., & Walker, D. (2015). How did hydraulic-fracturing operations in the Horn River Basin change seismicity patterns in northeastern British Columbia, Canada? *The Leading Edge*, *34*(6), 658–663. doi:10.1190/tle34060658.1

Farahbod, A. M., Kao, H., Walker, D. M., & Cassidy, J. F. (2015). Investigation of regional seismicity before and after hydraulic fracturing in the Horn River Basin, northeast British Columbia. *Canadian Journal of Earth Sciences*, *52*(2), 112–122. doi:10.1139/cjes-2014-0162

Font, Y., Kao, H., Lallemand, S., Liu, C. S., & Chiao, L. Y. (2004). Hypocentre determination offshore of eastern Taiwan using the maximum intersection method. *Geophysical Journal International*, *158*(2), 655–675. doi:10.1111/j.1365-246X.2004.02317.x

Johnson, J., & Slocomb, R. (2008). *INFORMATION #OGC 08-15: Regional Fields and Heritage Montney "A" Pool Mapping*. Fort St. John, BC. Retrieved from https://www.bcogc.ca/node/5531

Mahani, A. & Kao, H. (2019). Local magnitude scale for earthquakes in the Western Canada Sedimentary Basin, northeastern British Columbia and northwestern Alberta, in Geoscience BC Summary of Activities 2018: Energy and Water, Geoscience BC, Report2019-2, p. 47–54.

Mahani, A. B., Kao, H., Walker, D., Johnson, J., & Salas, C. (2016). Performance Evaluation of the Regional Seismograph Network in Northeast British Columbia, Canada, for Monitoring of Induced Seismicity. *Seismological Research Letters*, *87*(3), 648–660. doi:10.1785/0220150241

National Energy Board. (2013). *Energy Briefing Note: The Ultimate Potential for Unconventional Petroleum from the Montney Formation of British Columbia and Alberta*. Retrieved from https://www.neb-one.gc.ca/nrg/sttstc/ntrlgs/rprt/ltmtptntlmntnyfrmtn2013/ltmtptntlmntnyfrmtn2013-eng.pdf

Pavlis, G. L., Vernon, F., Harvey, D., & Quinlan, D. (2004). The generalized earthquake-location (GENLOC) package: An earthquake-location library. *Computers and Geosciences*, *30*(9–10), 1079–1091. doi:10.1016/j.cageo.2004.06.010

Richter, C. F. (1958). *Elemental Seismology*. San Francisco, California: W. H. Freeman and Co.

Richter, C. F. (1935). An instrumental earthquake magnitude scale. *Bulletin of the Seismological Society of America*, *25*(1), 1–32.

Ross, A., Padman, J., Sciences, A., & Isotope, S. (2014). Sharp increase in central Oklahoma seismicity since 2008 induced by massive wastewater injection. *Science*, *345*(6195), 448–451. doi:10.1126/science.1255802

Tan, F., Kao, H., Nissen, E., & Eaton, D. (2019). Seismicity-Scanning Based on Navigated Automatic Phase-Picking. *Journal of Geophysical Research: Solid Earth*, *124*(4), 3802–3818. doi:10.1029/2018JB017050

Visser, R., B. Smith, H. Kao, A. Babaie Mahani, J. Hutchinson, & J. McKay (2017). A comprehensive earthquake catalogue for northeastern British Columbia and western Alberta, 2014–2016, *Geol. Surv. Canada, Open File, 8335,* 28 pp., doi:10.4095/306292

Wessel, P., Smith, W. H. F., Scharroo, R., Luis, J., & Wobbe, F. (2013). Generic mapping tools: Improved version released. *Eos*, *94*(45), 409–410. doi:10.1002/2013EO450001

Wiemer, S., & Wyss, M. (2000). Minimum magnitude of completeness in earthquake catalogs: Examples from Alaska, the Western United States, and Japan. *Bulletin of the Seismological Society of America*, *90*(4), 859–869. doi:10.1785/0119990114

Yenier, E. (2017). A local magnitude relation for earthquakes in the Western Canada sedimentary Basin. *Bulletin of the Seismological Society of America*, *107*(3), 1421–1431. doi:10.1785/0120160275

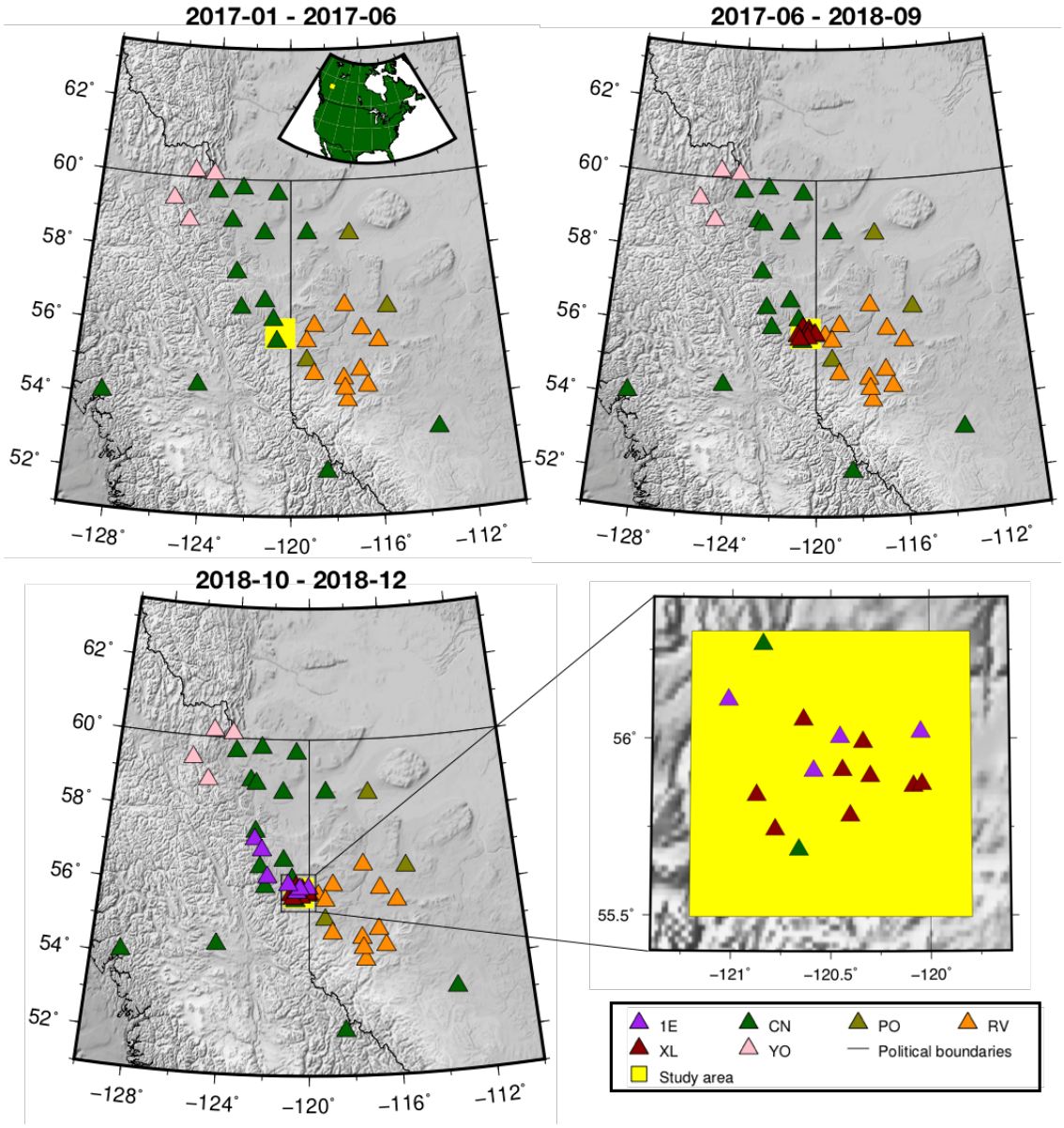


**Figure 1.** Distribution of seismic stations used in this study for the periods before XL network deployment (top-left panel), after XL network deployment but before 1E network deployment (top-right panel), after 1E network deployment (lower-left panel). The lower-right panel shows a zoomed-in view of the station coverage in the study area after 1E deployment. The black lines represent provincial and national borders.

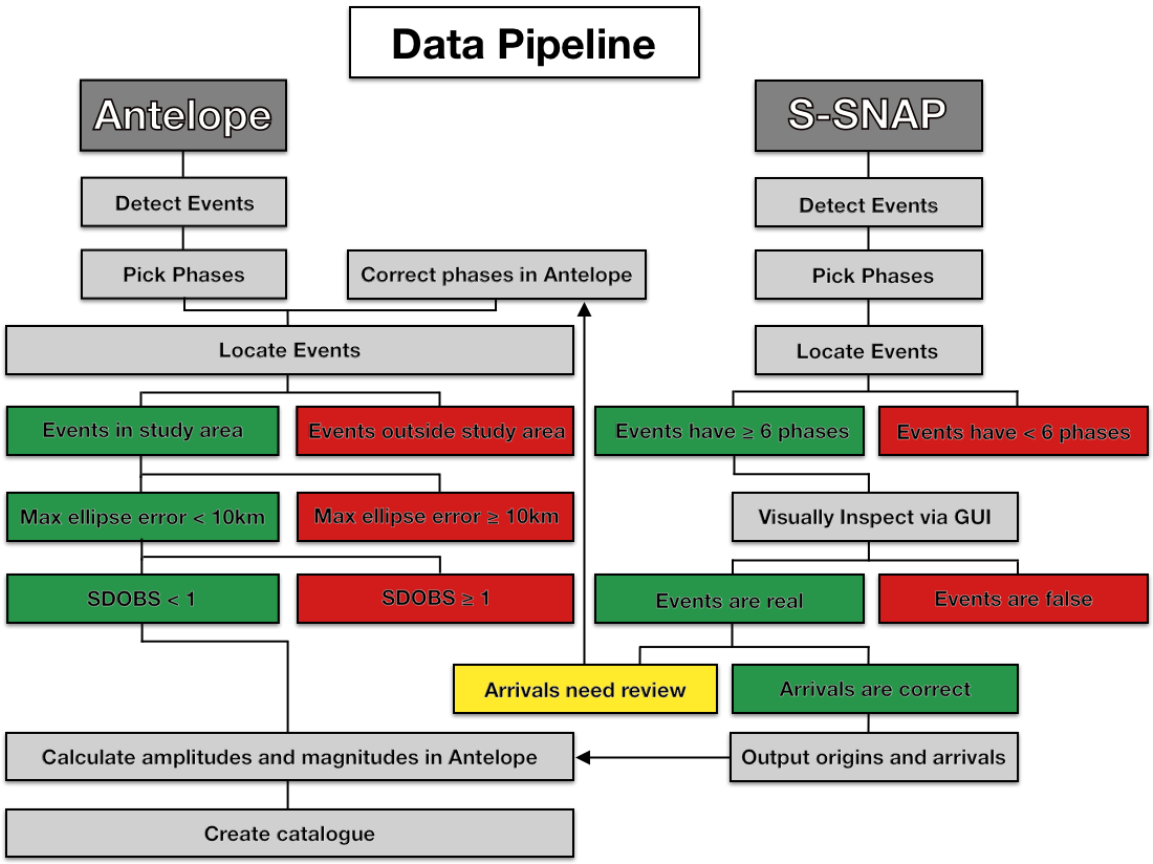


**Figure 2.** The data pipeline of the processes for completing the earthquake catalog with Antelope and S-SNAP. The pipeline flows along the black lines downwards unless indicated otherwise by an arrow. Green boxes mark criteria that must be met for an event in the pipeline to move forward. Red boxes mark criteria that remove events or arrivals that don't pass the quality control process and as a result will be removed. The yellow box indicates when an S-SNAP event and its arrivals are transferred to the Antelope location pipeline to be reviewed. Grey boxes indicate the actions to be taken.

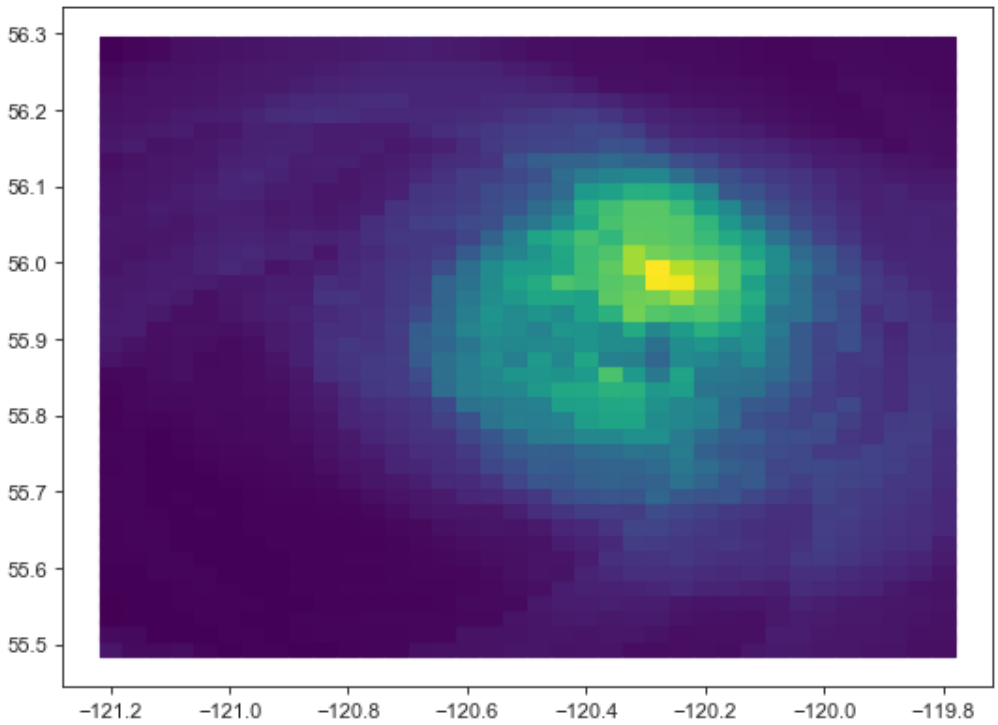


**Figure 3.** The image shows a map of brightness values at each scanned grid node of the study area at the time of a 1.5$M_L$ event (origin time: 2017-07-07 23:35:35). Brighter colours indicate higher brightness values which correspond to coherent arrivals of higher amplitudes and kurtosis peaks at all stations, typical of an earthquake. The cells in yellow in this case highlight the location where the event is most likely to have occurred; only the cell with the highest value is considered the source location which is used to determine the waveform segments at individual stations for precise determination of phase arrivals.

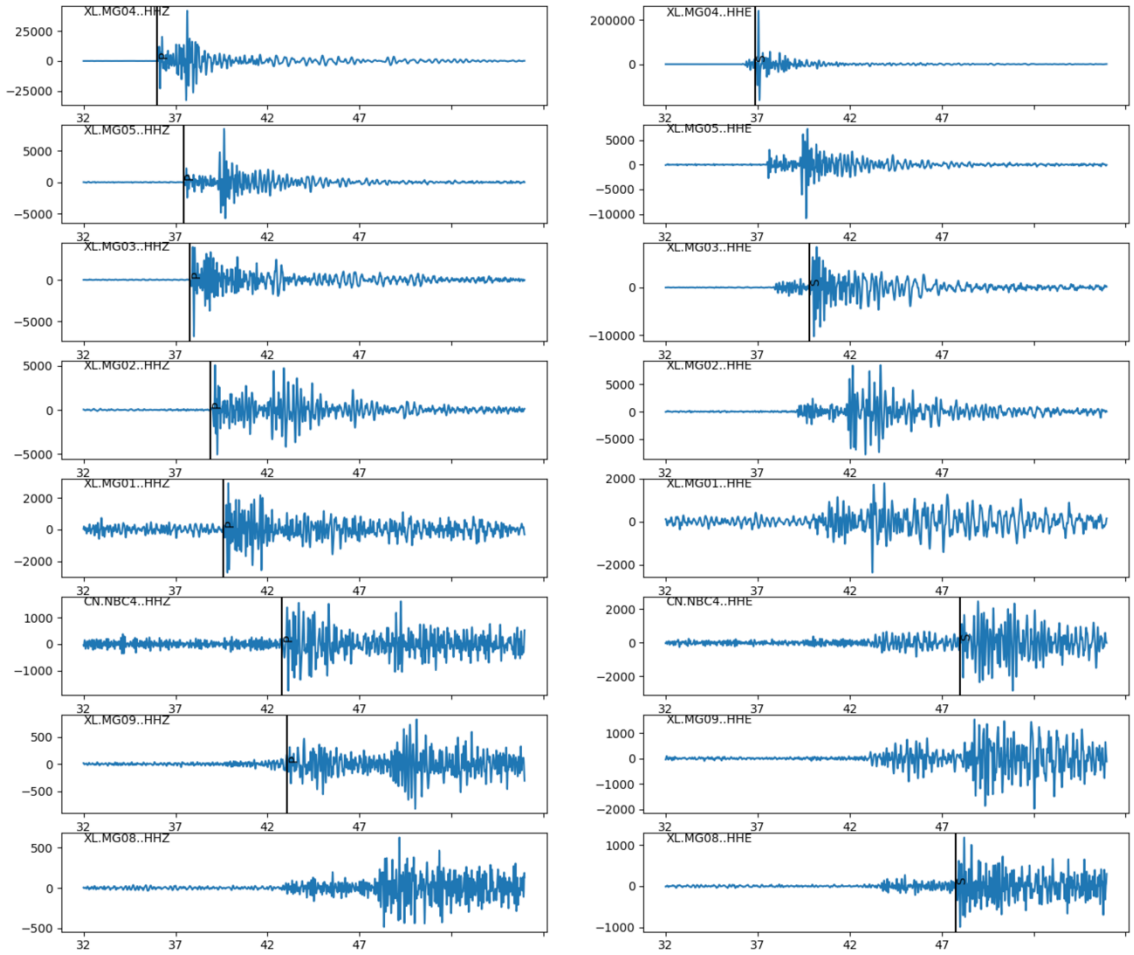


**Figure 4.** Screenshot of the Waveform Viewer GUI used to view waveforms and picks. This GUI allows an analyst to manually classify events as good, bad, or in need of review. The viewer sorts waveforms by P pick time first, then by S pick time. Waveforms are filtered using a 2-12 bandpass filter. Picks are shown as black lines, while waveform traces are shown in blue. The X-axis shows samples since the start of the time-window and the Y-axis for each trace shows the amplitude values after filtering. The event shown is a 1.5$M_L$ event that occurred 2017-07-07 23:35:35.

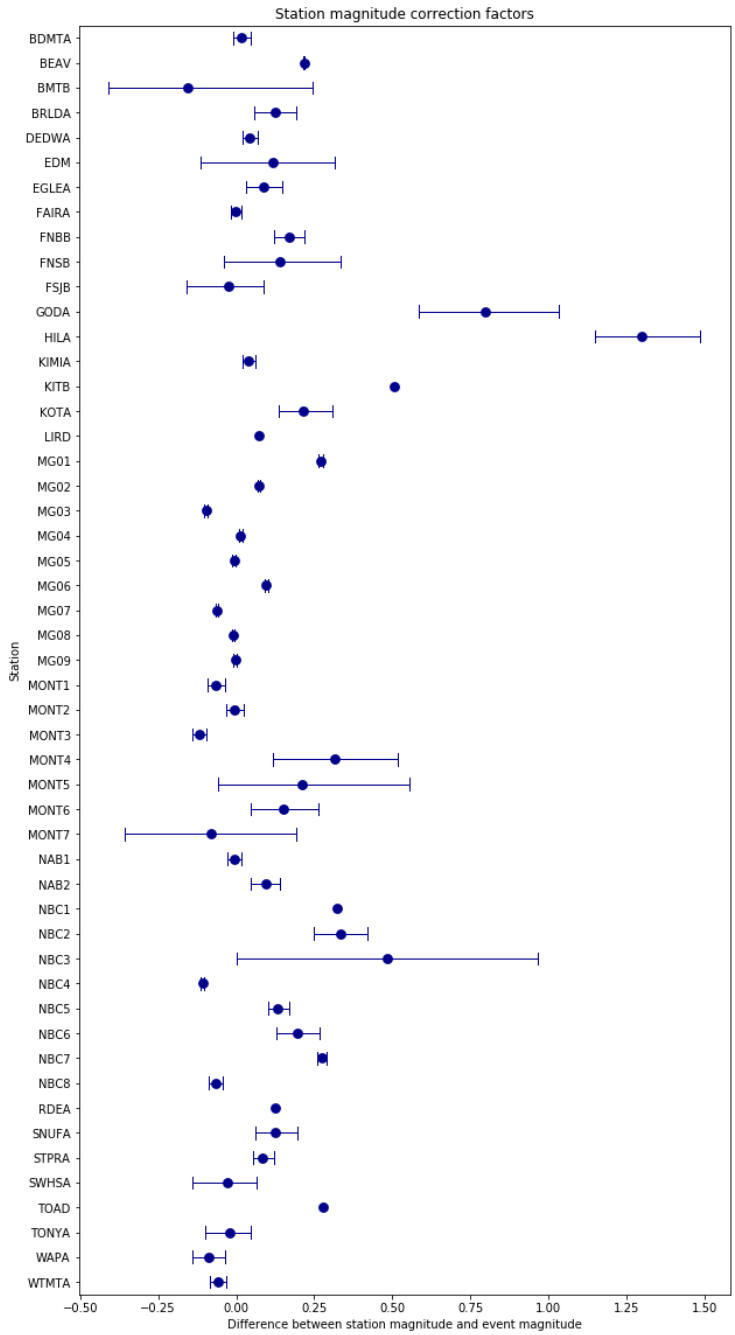


**Figure 5.** Station correction factors used in the magnitude calculation. For each station, the solid circle marks the average difference between station magnitudes and event magnitudes. Stations are sorted alphabetically. The thin lines with tails correspond to the 95$^{th}$ percentile of the sample distribution.

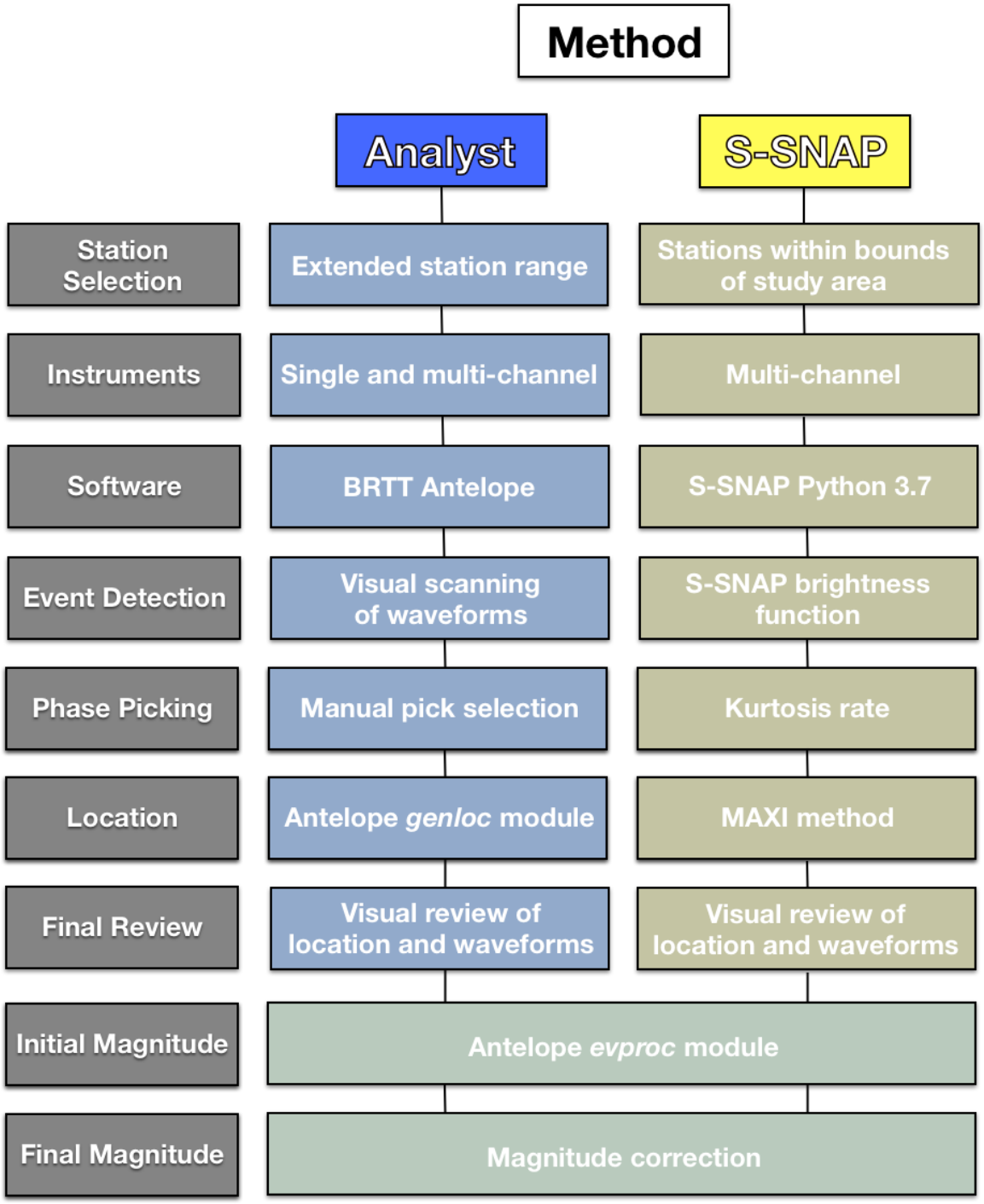


**Figure 6.** The settings and method to analyze events using manual analysis and with S-SNAP. The figure illustrates the key similarities and differences for each step performed by the analysts and S-SNAP.

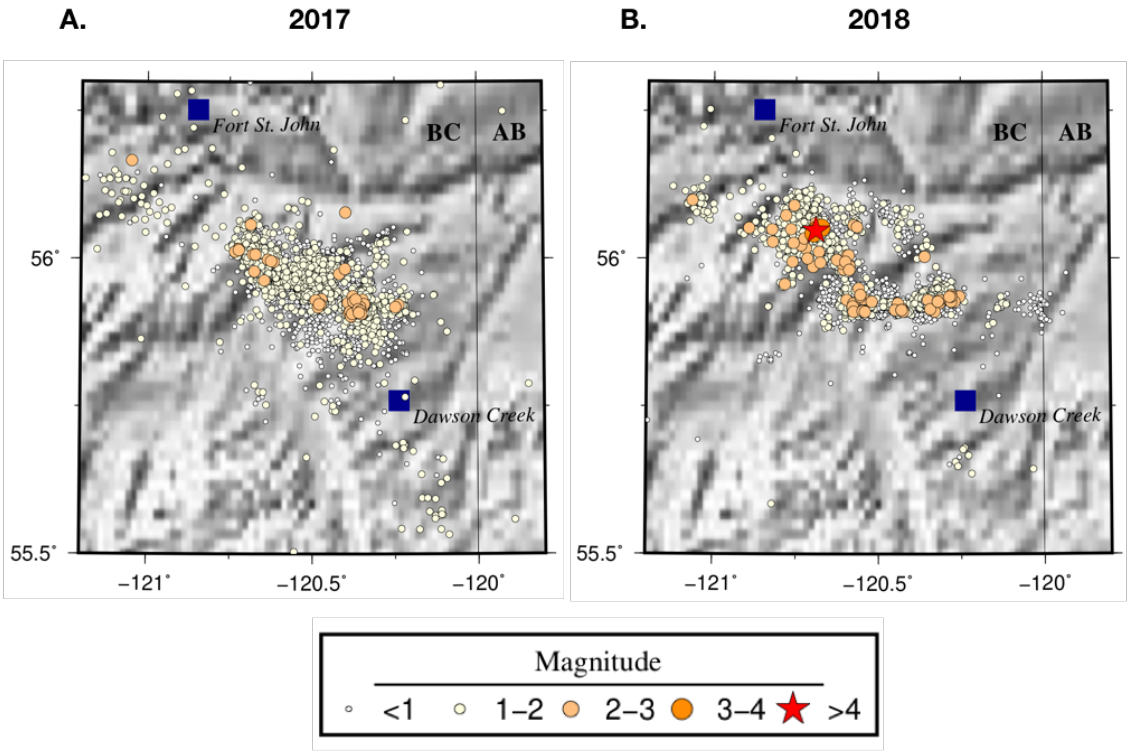


**Figure 7.** Maps showing the distribution of earthquakes in the study area during the time periods of 2017 (A) and 2018 (B). Black lines mark provincial boundaries. The sizes and colours of circles indicates the magnitude of the event. Blue squares indicate population centres.

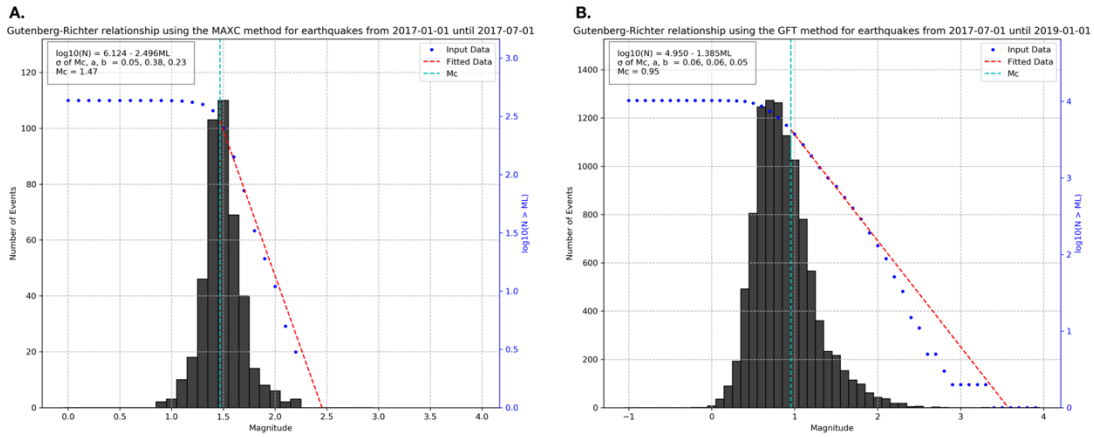


**Figure 8.** Magnitude of completeness plots for pre-XL network deployment, when there were only two stations available in the study area (A), and for the period afterwards when there were 10 or more stations (B).

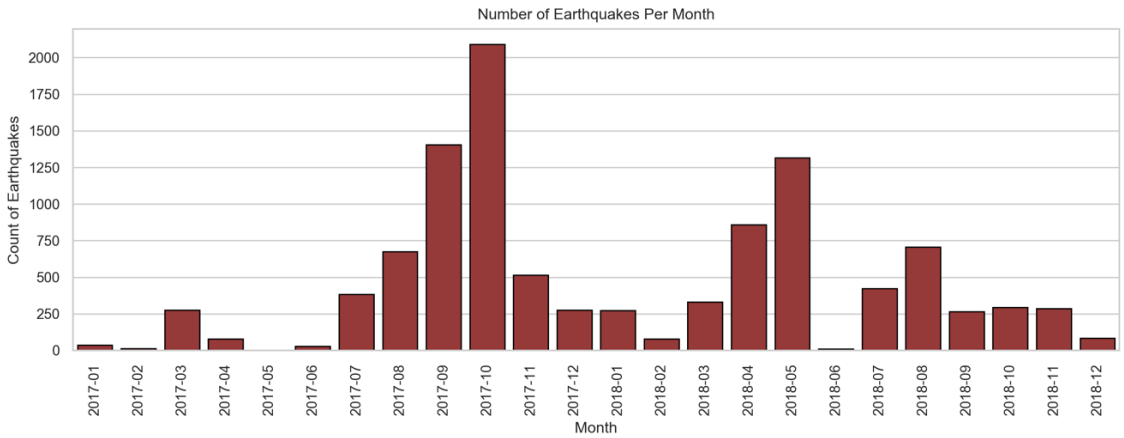


**Figure 9.** Histogram showing the number of earthquakes during each month of this study.

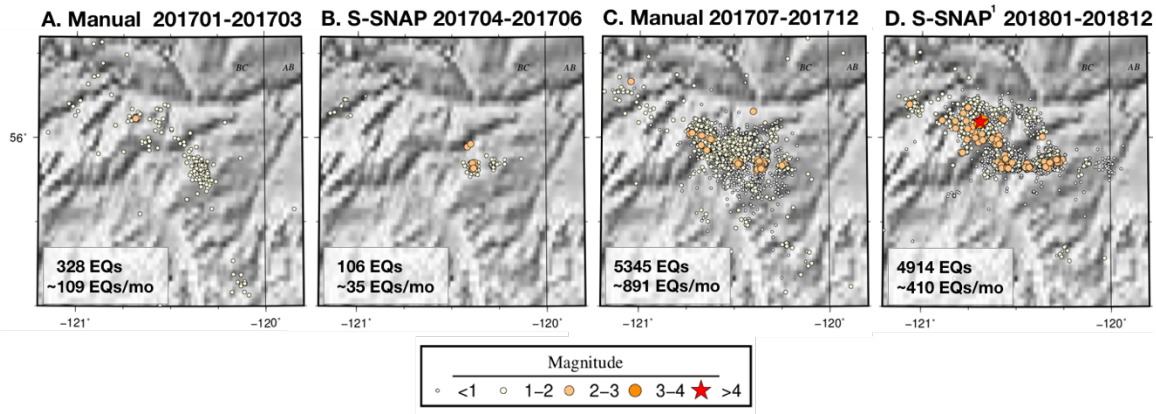


**Figure 10.** Maps showing the distribution of earthquakes for continuous time periods where the same location technique was used in northeastern BC and western AB. January 2017 through March 2017 was manually located (A), April 2017 through June 2017 events were located using S-SNAP (B), July 2017 through December 2017 events were manually located (C), and January 2018 through December 2018 events were located using S-SNAP (D). The map bounds constrain the study area. Black lines mark provincial boundaries. The size and colour of circles indicates the magnitude of the event. [1]Earthquakes from 22 Nov to 7 December 2018 were manually located in addition to being found by S-SNAP. For this period, when there were duplicated events the manually located solutions were preferred and S-SNAP events were discarded since manual locations used a higher number of stations and phases.

**Table 1.** List of Seismograph Stations Used in This Study.

| Network[1] | Station | Active Since[2] | Active Until | Latitude (˚N) | Longitude (˚E) | Instrument Type | Sampling Rate[3] |
|---|---|---|---|---|---|---|---|
| 1E | MONT1 | 2018274 | Present | 55.9102 | -120.5865 | Broadband | 100 |
| 1E | MONT2 | 2018274 | Present | 56.0197 | -120.047 | Broadband | 100 |
| 1E | MONT3 | 2018274 | Present | 56.0058 | -120.4539 | Broadband | 100 |
| 1E | MONT4 | 2018274 | Present | 57.3184 | -122.7057 | Broadband | 100 |
| 1E | MONT5 | 2018274 | Present | 57.0269 | -122.336 | Broadband | 100 |
| 1E | MONT6 | 2018276 | Present | 56.1103 | -121.017 | Broadband | 100 |
| 1E | MONT7 | 2018289 | Present | 56.3079 | -122.0316 | Broadband | 100 |
| CN | BMTB | 2017261 | Present | 56.0451 | -122.1332 | Broadband | 100 |
| CN | EDM | 1992155 | Present | 53.223 | -113.3497 | Broadband | 100 |
| CN | FNBB | 1999297 | 2017245 | 58.8903 | -123.0099 | Broadband | 100 |
| CN | FNSB | 2017214 | Present | 58.8061 | -122.7328 | Broadband | 100 |
| CN | FSJB | 2015308 | Present | 54.4588 | -124.2945 | Broadband | 100 |
| CN | KITB | 2014079 | Present | 54.0779 | -128.6368 | Broadband | 100 |
| CN | MNB | 1997168 | Present | 52.1976 | -118.3887 | Short-period | 100 |
| CN | NAB1 | 2014231 | Present | 56.7663 | -121.2587 | Broadband | 100 |
| CN | NAB2 | 2015244 | Present | 58.595 | -119.1656 | Broadband | 100 |
| CN | NBC1 | 2013060 | Present | 59.6559 | -123.8237 | Broadband | 100 |
| CN | NBC2 | 2013060 | Present | 59.7735 | -122.4878 | Broadband | 100 |
| CN | NBC3 | 2013060 | Present | 59.6372 | -120.6688 | Broadband | 100 |
| CN | NBC4 | 2013060 | Present | 55.6873 | -120.6602 | Broadband | 100 |
| CN | NBC5 | 2013060 | Present | 57.5231 | -122.6776 | Broadband | 100 |
| CN | NBC6 | 2013060 | Present | 58.5839 | -121.3339 | Broadband | 100 |
| CN | NBC7 | 2014222 | Present | 56.2678 | -120.8426 | Broadband | 100 |
| CN | NBC8 | 2016001 | Present | 56.5731 | -122.4044 | Broadband | 100 |
| RV | BDMTA | 2014227 | Present | 54.8129 | -118.9149 | Broadband | 100 |
| RV | BRLDA | 2014227 | Present | 54.092 | -117.4033 | Broadband | 100 |
| RV | DEDWA | 2016195 | Present | 56.6446 | -117.3891 | Broadband | 100 |
| RV | EGLEA | 2016195 | Present | 54.4571 | -116.4405 | Broadband | 100 |
| RV | FAIRA | 2016264 | Present | 56.1087 | -118.8648 | Broadband | 100 |
| RV | GODA | 2017205 | Present | 55.8392 | -119.5734 | Broadband | 100 |
| RV | HILA | 2014309 | Present | 58.5561 | -117.0203 | Broadband | 40 |
| RV | KIMIA | 2016265 | Present | 55.9938 | -116.6072 | Broadband | 100 |
| RV | RDEA | 2014310 | Present | 56.5513 | -115.3179 | Broadband | 100 |
| RV | SNUFA | 2016195 | Present | 54.6781 | -117.5398 | Broadband | 100 |
| RV | STPRA | 2014227 | Present | 55.6606 | -115.8323 | Broadband | 100 |
| RV | SWHSA | 2014227 | Present | 54.8994 | -116.7518 | Broadband | 100 |
| RV | TONYA | 2016237 | Present | 54.4054 | -117.4908 | Broadband | 100 |
| RV | WAPA | 2014314 | Present | 55.1833 | -119.2536 | Broadband | 40 |
| RV | WTMTA | 2014227 | Present | 55.6942 | -119.2398 | Broadband | 100 |
| XL | MG01 | 2017170 | Present | 56.0548 | -120.638 | Broadband | 100 |
| XL | MG02 | 2017165 | Present | 55.8668 | -120.084 | Broadband | 100 |
| XL | MG03 | 2017167 | Present | 55.9122 | -120.4414 | Broadband | 100 |
| XL | MG04 | 2017168 | Present | 55.9914 | -120.338 | Broadband | 100 |
| XL | MG05 | 2017166 | Present | 55.8951 | -120.3019 | Broadband | 100 |
| XL | MG06 | 2018173 | Present | 55.8721 | -120.0415 | Broadband | 100 |
| XL | MG07 | 2017214 | Present | 55.7836 | -120.4024 | Broadband | 100 |
| XL | MG08 | 2017165 | Present | 55.8412 | -120.8731 | Broadband | 100 |
| XL | MG09 | 2017169 | Present | 55.7442 | -120.7796 | Broadband | 100 |
| YO | BEAV | 2016173 | Present | 60.1798 | -125.0684 | Broadband | 100 |
| YO | KOTA | 2016173 | Present | 60.1301 | -124.0527 | Broadband | 100 |
| YO | LIRD | 2016163 | Present | 59.4098 | -126.0986 | Broadband | 100 |
| YO | TOAD | 2016165 | Present | 58.8499 | -125.2333 | Broadband | 100 |

[1] CN: Canadian National Seismograph Network, RV: Regional Alberta Observatory for Earthquake Studies Network), TD: TransAlta Monitoring Network, NY: Yukon-Northwest Seismic Network. Stations are sorted firstly by 'Network,' and secondly by 'Active Since.'

[2] Year (4-digit) and Julian day (3-digit).

[3] Sampling rate is in number of samples per second.

**Table 2.** List of Station Magnitude Correction Factors

| Station Name* | Correction Factor | No. of Events |
|---|---|---|
| BDMTA | 0.021 | 298 |
| BEAV | 0.127 | 2 |
| BMTB | -0.166 | 8 |
| BRLDA | 0.110 | 27 |
| DEDWA | 0.039 | 292 |
| EDM | 0.024 | 3 |
| EGLEA | 0.063 | 14 |
| FAIRA | -0.001 | 605 |
| FNBB | 0.118 | 31 |
| FNSB | 0.063 | 5 |
| FSJB | -0.049 | 9 |
| GODA | 0.794 | 24 |
| HILA | 1.253 | 6 |
| KIMIA | 0.033 | 190 |
| KITB | 0.394 | 1 |
| KOTA | 0.126 | 4 |
| LIRD | 0.000 | 1 |
| MG01 | 0.278 | 5122 |
| MG02 | 0.079 | 6582 |
| MG03 | -0.105 | 9223 |
| MG04 | 0.029 | 5224 |
| MG05 | 0.003 | 8416 |
| MG06 | 0.096 | 1496 |
| MG07 | -0.067 | 7059 |
| MG08 | -0.011 | 5575 |
| MG09 | -0.006 | 4261 |
| MONT1 | -0.093 | 178 |
| MONT2 | 0.016 | 103 |
| MONT3 | -0.107 | 140 |
| MONT4 | 0.275 | 27 |
| MONT5 | 0.200 | 16 |
| MONT6 | 0.248 | 20 |
| MONT7 | -0.156 | 2 |
| NAB1 | -0.006 | 179 |
| NAB2 | 0.071 | 12 |
| NBC1 | 0.256 | 1 |
| NBC2 | 0.259 | 7 |
| NBC3 | 0.429 | 2 |
| NBC4 | -0.108 | 4543 |
| NBC5 | 0.126 | 263 |
| NBC6 | 0.187 | 46 |
| NBC7 | 0.278 | 1897 |
| NBC8 | -0.067 | 387 |
| RDEA | 0.115 | 1 |
| SNUFA | 0.113 | 41 |
| STPRA | 0.059 | 51 |
| SWHSA | -0.047 | 3 |
| TOAD | 0.164 | 1 |
| TONYA | -0.009 | 11 |
| WAPA | -0.077 | 121 |
| WTMTA | -0.047 | 374 |

*Stations are sorted alphabetically.

**Appendix 1.** Regional Earthquake Catalogue for the Fort St. John – Dawson Creek Area (1 January 2017 – 31 December 2018)

Appendix 1 lists all seismic events included in the final version of our earthquake catalogue. It is given as an Excel spreadsheet for easy data manipulation. The event origins with the Auth codes, "analyst," and "ssnap-analyst" were determined using the software program *genloc* (Pavlis et al., 2004) while origins with the auth code ssnap were determined using S-SNAP. Magnitudes were determined by the Antelope module, *evproc*, part of the *Antelope 5.7* software suite. There are 17 columns and the corresponding parameters are:

| | | |
|---|---|---|
| lat | **(Float)**: | The latitude of the origin in decimal degrees north. Given to 4 decimal places. |
| lon | **(Float)**: | The longitude of the origin in decimal degrees east. Given to 4 decimal places. |
| depth | **(Float)**: | The depth of the origin in km. Given to 1 decimal place. |
| datetime | (**Datetime**): | The date and time combined in datetime format. Given to 3 decimal places. |
| mag | **(Float)**: | The magnitude of the origin. Given to 1 decimal place. |
| magtype | (**String**): | The magnitude type for the mag value in the same row. Possible values are ML or MW. MW values were input for events with moment tensor solutions from the CNSN catalogue. |
| cmag | **(Float)**: | The corrected magnitude of the origin. Given to 1 decimal place. |
| cmagtype | (**String**): | The corrected magnitude type for the cmag value in the same row. Possible values are ML or MW. MW values were input for events with moment tensor solutions from the CNSN catalogue. |
| ndef | (**Int**): | The number of phases used to locate the origin. |
| sdobs | **(Float)**: | The standard deviation of travel time residuals. Null for S-SNAP locations. Given to 2 decimal places. |
| smajax | **(Float)**: | The major axis length in km of the error ellipse as determined by *genloc*. Null for S-SNAP locations. Given to 2 decimal places. |
| sminax | **(Float)**: | The minor axis length in km of the error ellipse as determined by *genloc*. Null for S-SNAP locations. Given to 2 decimal places. |
| sdepth | **(Float)**: | The depth axis length in km of the error ellipse as determined by *genloc*. Null for S-SNAP locations. Given to 2 decimal places. |
| fixed_depth | (**Int**): | Whether the depth of the origin was manually fixed by the analyst during analysis or not. Possible values are 'Y', or 'N', or Null for S-SNAP locations. |
| strike | **(Float)**: | The strike of the major axis of the error ellipse as determined by *genloc*. Null for S-SNAP locations. Given to 1 decimal place. |
| auth | (**String**): | The author location method of the origin. Possible values include analyst, ssnap-analyst, or ssnap. |
| orid | (**Int**): | The unique origin ID of the origin. |

**Appendix 2.** Arrival Picks for Seismic Events Listed in Appendix 1.

Appendix 2 lists all arrivals for events included in the final version of our earthquake catalogue. It is formatted as an Excel spreadsheet. There are 8 columns and the corresponding parameters are:

| | | |
|---|---|---|
| sta | (**String**): | The station on which the phase pick was chosen. |
| chan | (**String**): | The channel on which the phase pick was chosen. |
| phase | (**String**): | The phase picked. Possible options include *P, S, Pn, Pg, Sn,* or *Sg*. |
| datetime | (**Datetime**): | The date and time of the phase pick. Given to 3 decimal places. |
| delta | **(Float)**: | The arc length of the path that the seismic signal travels from source to receiver. Null for S-SNAP arrivals. Given to 3 decimal places. |
| timeres | **(Float)**: | The time difference in seconds between the theoretical phase arrival and when it was picked. Null for S-SNAP arrivals. Given to 3 decimal places. |
| wgt | **(Float)**: | The final weight output onto the arrival by the location algorithm. Can be any value from 0 to 1. Null for S-SNAP arrivals. Given to 3 decimal places. |
| orid | (**Int**): | The origin ID that the arrivals belong to. |

**Appendix 3.** Magnitudes for Seismic Events Listed in Appendix 1.

Appendix 3 lists all station magnitudes for events included in the final version of our earthquake catalogue. It is formatted as an Excel spreadsheet. There are 7 columns and the corresponding parameters are:

| | | |
|---|---|---|
| sta | (**String**): | The station on which the magnitude was calculated. |
| chan | (**String**): | The channel on which the magnitude was calculated. |
| datetime | (**Datetime**): | The date and time of the magnitude calculation. Given to 3 decimal places. |
| amp | (**Float**): | The amplitude value calculated on the station and channel at the given datetime by the Antelope module *evproc*. Given to 3 decimal places. |
| ml | (**Float**): | The raw station magnitude as determined by the Antelope module *evproc*. Given to 2 decimal places. |
| cml | (**Float**): | The corrected station magnitude. Given to two decimal places. |
| orid | (**Int**): | The origin ID that the magnitudes belong to. |